Inorg. Chem. **2009**, *48*, 2887−2898

$[M^{III}(dmit)_2]^-$-Coordinated Mn^{III} Salen-Type Dimers (M^{III} = Ni^{III}, Au^{III}; $dmit^{2-}$ = 1,3-Dithiol-2-thione-4,5-dithiolate): Design of Single-Component Conducting Single-Molecule Magnet-Based Materials

Hiroki Hiraga,[†] Hitoshi Miyasaka,*[,†] Rodolphe Clérac,[‡,§] Marc Fourmigué,[||] and Masahiro Yamashita[†]

Department of Chemistry, Graduate School of Science, Tohoku University, 6-3 Aramaki-Aza-Aoba, Aoba-ku, Sendai, Miyagi 980-8578, Japan, CNRS, UPR 8641, Centre de Recherche Paul Pascal (CRPP), Equipe "Matériaux Moléculaires Magnétiques", 115 avenue du Dr. Albert Schweitzer, Pessac F-33600, France, Université de Bordeaux, UPR 8641, Pessac F-33600, France, and Sciences Chimiques de Rennes, Université Rennes 1, UMR CNRS 6226, Campus de Beaulieu, 35042 Rennes, France

Received November 5, 2008

Four linear-type tetranuclear complexes, $[Mn(5\text{-}Rsaltmen)\{M(dmit)_2\}]_2$ (R = MeO, M = Ni, **1a**; M = Au, **1b**; R = Me, M = Ni, **2a**; M = Au, **2b**), were synthesized and structurally characterized (5-Rsaltmen^{2-} = *N*,*N*′-(1,1,2,2-tetramethylethylene)-bis(5-Rsalicylideneiminate), $dmit^{2-}$ = 1,3-dithiol-2-thione-4,5-dithiolate). These compounds crystallize in the same triclinic $P\bar{1}$ space group ($Z = 1$) and have a similar molecular structure with a bridging array of $[M-(dmit)-Mn-(O_{Ph})_2-Mn-(dmit)-M]$ and a packing feature where the respective sets of **1a**/**1b** and **2a**/**2b** are isomorphous. Intermolecular $\pi-\pi$/S···S contacts are observed between the coordinating $[M(dmit)_2]^-$ moieties to form zigzag stair-like columns along the *a* axis direction. Hückel calculations revealed a strong intermolecular dimerization within the $[Ni(dmit)_2]^-$ column that makes them magnetically silent even at room temperature. Nevertheless, **1a** and **2a** with M = Ni behave as semiconductors with $\sigma_{r.t.} = 7 \times 10^{-4}$ S·cm^{-1} and $E_a = 182$ meV for **1a** and $\sigma_{r.t.} = 1 \times 10^{-4}$ S·cm^{-1} and $E_a = 292$ meV for **2a**, while **1b** and **2b** with M = Au are insulators. As a result of the strong dimerization of the $[Ni(dmit)_2]^-$ anions, the magnetic properties of **1a** are essentially identical to those of **1b** and **2b**, which can be described as isolated Mn(III) dimers, acting as single-molecule magnets (SMM). Meanwhile, the magnetic properties of **2a** are dominated by the intermolecular Mn···Mn antiferromagnetic interactions via the singlet $[Ni(dmit)_2]_2^{2-}$ dimer ($J_{Mn\cdots Mn}/k_B = -2.85$ K), inducing a long-range antiferromagnetic order at $T_N = 6.4$ K. The present systems are unique materials made of neutral single-component complexes that exhibit two major solid-state properties, that is, electrical conductivity and magnetism, varied as semiconductor/SMM for **1a**, insulator/SMM for **1b** and **2b**, and semiconductor/antiferromagnet for **2a** by tuning metal center and partial structural modification.

Introduction

Since the discovery of polymetallic complexes exhibiting the slow relaxation of magnetization, the so-called single-molecule magnets (SMMs), in the beginning of 1990s,[1] a large number of such complexes have been synthesized by the bottom-up synthetic approach. In addition to the design of unique SMMs, the tuning of slow dynamics and quantum properties such as quantum tunneling of magnetization (QTM) is nowadays one of the most active themes of research in this field. One way to design molecules to tune such properties is to control inter-SMM interactions that perturb not only the QTM but also the thermally activated slow dynamics of magnetization.[2] A good example of such effects can be seen in dimers of antiferromagnetically coupled

* To whom correspondence should be addressed. E-mail: miyasaka@agnus.chem.tohoku.ac.jp. Fax: (+81)22-795-6548.
† Tohoku University.
‡ CRPP.
§ Université de Bordeaux.
|| Université Rennes 1.

(1) Sessoli, R.; Tsai, H.-L.; Schake, A. R.; Wang, S.; Vincent, J. B.; Folting, K.; Gatteschi, D.; Christou, G.; Hendrickson, D. N. *J. Am. Chem. Soc.* **1993**, *115*, 1804.

(2) Miyasaka, H.; Yamashita, M. *Dalton Trans.* **2007**, 399.

10.1021/ic802110b CCC: $40.75
Published on Web 03/02/2009

$[Mn_4]$ SMMs synthesized by Hendrickson et al.[3] In this compound, exchange-bias QTM and quantum coherence are observed,[4,5] showing that the supramolecular dimer of SMMs exhibits dramatically different dynamics than the isolated $[Mn_4]$ SMM. Another example of inter-SMM interaction effects is found in one-dimensional (1D) systems of SMMs, like the single-chain magnet (SCM) systems,[6−8] or the chains of antiferromagnetically coupled SMMs,[9,10] in which the characteristic energies of the dynamics are functions of inter-SMM exchanges.[11] Also in the SCM systems, the presence of one-dimensional correlations does not rule out the presence of unique quantum effects, as shown by the reversal of the magnetization at low temperatures that is induced by a quantum nucleation of a domain wall.[12]

Another interesting strategy toward the tuning and modification of SMM characteristics is to design multifunctional molecules,[13] in which other properties such as electron-transfer phenomenon, electrical conductivity, dielectric property,[13d] spin-crossover behavior, and so forth would be targets in synergy with the SMM behavior. However, such SMM-based hybrid systems have never been reported so far because of the difficulty in associating the desired functional building units in such a way that they interact. Hence, it is becoming of great importance for this field of research to find useful approaches for the molecular design of these polyfunctional systems. As far as we know, only two relevant reports by our group have been published, in which hybrid materials exhibiting SMM behavior with a simple addition of the second physical property, electrical conductivity, were described.[2] The first example, $[\{Mn^{II}_2Mn^{III}_2(hmp)_6(MeCN)_2\}\{Pt(mnt)_2\}_4][Pt(mnt)_2]_2$ ($hmp^- =$ 2-hydroxymethylpyridinate, $mnt^{2-} =$ maleonitriledithiolate), has been synthesized electrochemically in a solution containing functional building blocks, $[Mn^{II}_2Mn^{III}_2(hmp)_6(MeCN)_2(H_2O)_4](ClO_4)_4$ and $(NBu_4)[Pt(mnt)_2]$.[14] This material behaves as an SMM and also possesses semiconductor properties, thanks to the network of mixed-valent $[Pt(mnt)_2]^{n-}$ stacks. In addition, four $[Pt(mnt)_2]^{n-}$ molecules coordinated to the SMM moiety to form a unique $[\{Mn^{II}_2Mn^{III}_2(hmp)_6(MeCN)_2\}\{Pt(mnt)_2\}_4]^{m-}$ SMM unit. Unfortunately, no significant electronic interaction between the SMM unit and the conducting column was observed. More recently, the second example has been synthesized from a series of Mn(III) dinuclear SMMs, $[Mn^{III}_2(5\text{-MeOsaltmen})_2(solv)_2]^{2+}$ ($5\text{-MeOsaltmen}^{2-} = N,N'$-(1,1,2,2-tetramethylethylene)-bis(5-methoxysalicylideneiminate); solv = acetone or acetonitrile), and $[Ni(dmit)_2]^{n-}$ anions ($dmit^{2-} =$ 1,3-dithiol-2-thione-4,5-dithiolate): $[Mn_2(5\text{-MeOsaltmen})_2(solv)_2][Ni(dmit)_2]_7\cdot 4(solv)$.[15] Even making an aggregated structure comprising two-component layers, the complete separation of two components in the final crystal structure led to independent electrical and magnetic properties as a semiconductor and a SMM, but it is worth mentioning that the electrical conductivity at room temperature was increased by a factor of 10 ($\sigma_{r.t.} \approx 2\ S\cdot cm^{-1}$) in comparison to the first example, thanks to the use of $[Ni(dmit)_2]^{n-}$.

Following these new synthetic strategies toward SMM-based polyfunctional materials with a synergy of electrical and magnetic properties, we present in this paper a new class of conducting and magnetic materials: $[Mn^{III}(5\text{-Rsaltmen})\{M^{III}(dmit)_2\}]_2$ (R = MeO, M^{III} = Ni, **1a**; M^{III} = Au, **1b**; R = Me, M^{III} = Ni, **2a**; M^{III} = Au, **2b**). These compounds have a simple Mn(III) saltmen out-of-plane dinuclear core of formula, $[Mn^{III}(5\text{-Rsaltmen})(X)]_2$, where X^- is a coordinating counteranion corresponding to $[M^{III}(dmit)_2]^-$ in the present compounds. Since the coordinating $[M^{III}(dmit)_2]^-$ moiety is a monoanion, these compounds consist of a single-component neutral unit having a linear tetranuclear $[M^{III}-Mn^{III}-Mn^{III}-M^{III}]$ skeleton. Intermolecular contacts of the $[Ni^{III}(dmit)_2]^-$ ($S = 1/2$) moieties in **1a** and **2a** induce a strong spin dimerization that makes them magnetically silent even at room temperature. Nevertheless, **1a** and **2a** exhibit semiconducting properties, while **1b** and **2b** behave as electrical insulators, as expected in the presence of diamagnetic $[Au^{III}(dmit)_2]^-$ anions. Interestingly, the magnetic properties of **1a** and **2a** are completely different despite their similar structures; as we will see, **1a**, **1b**, and **2b** behave as SMMs because of the good magnetic isolation provided by the $[M^{III}(dmit)_2]^-$ column acting only as a magnetic buffer layer, while **2a** exhibits an antiferromagnetic three-dimensional order induced by a significant intermolecular Mn···Mn exchange through the singlet $[Ni^{III}(dmit)_2]_2^{2-}$ dimer that makes the semiconductor network. The present series of

(3) Hendrickson, D. N.; Christou, G.; Schmitt, E. A.; Libby, E.; Bashkin, J. S.; Wang, S.; Tsai, H.-L.; Vincent, J. B.; Boyd, P. D.; Huffman, J. C.; Folting, K.; Li, Q.; Streib, W. E. *J. Am. Chem. Soc.* **1992**, *114*, 2455.

(4) Wernsdorfer, W.; Aliaga-Alcalde, N.; Hendrickson, D. N.; Christou, G. *Nature* **2002**, *416*, 406.

(5) Hill, S.; Edwards, R. S.; Aliaga-Alcalde, N.; Christou, G. *Science* **2003**, *302*, 1015.

(6) Clérac, R.; Miyasaka, H.; Yamashita, M.; Coulon, C. *J. Am. Chem. Soc.* **2002**, *124*, 12837.

(7) (a) Miyasaka, H.; Clérac, R.; Mizushima, K.; Sugiura, K.; Yamashita, M.; Wernsdorfer, W.; Coulon, C. *Inorg. Chem.* **2003**, *42*, 8203. (b) Miyasaka, H.; Nezu, T.; Sugimoto, K.; Sugiura, K.; Yamashita, M.; Clérac, R. *Chem.—Eur. J.* **2005**, *11*, 1592. (c) Saitoh, A.; Miyasaka, H.; Yamashita, M.; Clérac, R. *J. Mater. Chem.* **2007**, *17*, 2002.

(8) Ferbinteanu, M.; Miyasaka, H.; Wernsdorfer, W.; Nakata, K.; Sugiura, K.; Yamashita, M.; Coulon, C.; Clérac, R. *J. Am. Chem. Soc.* **2005**, *127*, 3090.

(9) Lecren, L.; Wernsdorfer, W.; Li, Y.-G.; Vindigni, A.; Miyasaka, H.; Clérac, R. *J. Am. Chem. Soc.* **2007**, *129*, 5045.

(10) (a) Lecren, L.; Roubeau, O.; Coulon, C.; Li, Y.-G.; Le Goff, X. F.; Wernsdorfer, W.; Miyasaka, H.; Clérac, R. *J. Am. Chem. Soc.* **2005**, *127*, 17353. (b) Lecren, L.; Roubeau, O.; Li, Y.-G.; Le Goff, X. F.; Miyaska, H.; Richard, F.; Wernsdorfer, W.; Coulon, C.; Clérac, R. *Dalton Trans.* **2008**, 755.

(11) (a) Coulon, C.; Clérac, R.; Lecren, L.; Wernsdorfer, W.; Miyasaka, H. *Phys. Rev. B* **2004**, *69*, 132408. (b) Coulon, C.; Miyasaka, H.; Clérac, R. *Struct. Bonding (Berlin, Ger.)* **2006**, *122*, 163. (c) Coulon, C.; Clérac, R.; Wernsdorfer, W.; Colin, T.; Saitoh, A.; Motokawa, N.; Miyasaka, H. *Phys. Rev. B* **2007**, *76*, 214422.

(12) Wernsdorfer, W.; Clérac, R.; Coulon, C.; Lecren, L.; Miyasaka, H. *Phys. Rev. Lett.* **2005**, *95*, 237203.

(13) (a) Coronado, E.; Day, P. *Chem. Rev.* **2004**, *104*, 5419. (b) Coronado, E.; Galán-Mascarós, J. R.; Gómez-Garcia, C. J.; Laukhin, V. *Nature* **2000**, *408*, 447. (c) Uji, S.; Shinagawa, H.; Terashima, T.; Yakabe, T.; Terai, Y.; Tokumoto, M.; Kobayashi, A.; Tanaka, H.; Kobayashi, H. *Nature* **2001**, *410*, 908. (d) Bai, Y.-L.; Tao, J.; Wernsdorfer, W.; Sato, O.; Huang, R.-B.; Zhang, L.-S. *J. Am. Chem. Soc.* **2006**, *128*, 16428. (e) Takahashi, K.; Cui, H.-B.; Okano, Y.; Kobayashi, H.; Mori, H.; Tajima, H.; Einaga, Y.; Sato, O. *J. Am. Chem. Soc.* **2008**, *130*, 6688.

(14) Hiraga, H.; Miyasaka, H.; Nakata, K.; Kajiwara, T.; Takaishi, S.; Oshima, Y.; Nojiri, H.; Yamashita, M. *Inorg. Chem.* **2007**, *46*, 9661.

(15) Hiraga, H.; Miyasaka, H.; Takaishi, S.; Kajiwara, T.; Yamashita, M. *Inorg. Chim. Acta* **2008**, *361*, 3863.

materials is a unique case in which a single-component molecule displays various electrical and magnetic properties such as semiconductor/SMM (**1a**), insulator/SMM (**1b** and **2b**), and semiconductor/antiferromagnet (**2a**).[16] The syntheses, crystal structures, electrical conductivity, and magnetic properties of these compounds are reported.

Experimental Section

General Procedures and Materials. All syntheses were carried out under an aerobic condition, and solvents were used without further purification. The starting materials, $[Mn_2(5\text{-MeOsaltmen})_2(H_2O)_2](PF_6)_2$ and $[Mn_2(5\text{-Mesaltmen})_2(H_2O)_2](PF_6)_2$, were prepared according to the literature.[17] $(NBu_4)[M(dmit)_2]$ was prepared following the previously reported method.[18,19]

$[Mn(5\text{-MeOsaltmen})\{Ni(dmit)_2\}]_2$ (1a). To an acetone solution (4 mL) of $[Mn^{III}_2(5\text{-MeOsaltmen})_2(H_2O)_2](PF_6)_2$ (6 mg, 0.005 mmol) was added an acetone solution (4 mL) of $(NBu_4)[Ni(dmit)_2]$ (6.9 mg, 0.01 mmol), and then, the mixture was stirred for several minutes at room temperature to produce a dark green solution. This solution was added with 4 mL of 2-propanol and was kept, undisturbed, for 3 days at room temperature to yield black block-shaped crystals of **1a**. The obtained crystal sample was, just in case, washed with a small amount of $CHCl_3$ and MeOH to remove the starting materials which might be slightly recrystallized. 7.12 mg, 80%. Calcd for $C_{56}H_{52}Mn_2N_4O_8Ni_2S_{20}$ (**1a**): C, 37.84; H, 2.95; N, 3.15. Found: C, 38.11; H, 3.12; N, 3.12. IR (KBr pellet, cm^{-1}): 1591, 1537, 1463, 1387, 1348, 1319, 1290, 1228, 1199, 1168, 1141, 1060, 1020, 827, 759.

$[Mn(5\text{-MeOsaltmen})\{Au(dmit)_2\}]_2$ (1b). To an acetone solution (1 mL) of $[Mn^{III}_2(5\text{-MeOsaltmen})_2(H_2O)_2](PF_6)_2$ (3 mg, 0.0025 mmol) was added an acetone solution (1 mL) of $(NBu_4)[Au(dmit)_2]$ (4.16 mg, 0.005 mmol), and then, the mixture was stirred for several minutes at room temperature to produce a brown solution. This solution was added with 1 mL of toluene and was kept, undisturbed, for 1 day at room temperature to yield black block-shaped crystals of **1b**. The obtained crystal sample was, just in case, washed with a small amount of $CHCl_3$ and MeOH to remove the starting materials which might be slightly recrystallized. 3.35 mg, 66%. Calcd for $C_{56}H_{52}Mn_2N_4O_8Au_2S_{20}$ (**1b**): C, 32.74; H, 2.55; N, 2.73. Found: C, 32.88; H, 2.68; N, 2.70. IR (KBr pellet, cm^{-1}): 1619, 1591, 1541, 1466, 1358, 1290, 1228, 1199, 1168, 1145, 1063, 1029, 827, 759.

$[Mn(5\text{-Mesaltmen})\{Ni(dmit)_2\}]_2$ (2a). To an acetone solution (4 mL) of $[Mn^{III}_2(5\text{-Mesaltmen})_2(H_2O)_2](PF_6)_2$ (5.68 mg, 0.005 mmol) was added an acetone solution (4 mL) of $(NBu_4)[Ni(dmit)_2]$ (6.9 mg, 0.01 mmol), and then, the mixture was stirred for several minutes at room temperature to produce a dark green solution. After 4 mL of toluene was added, this solution was divided into two portions and was kept, undisturbed, for 2 days at room temperature to yield black block-shaped crystals of **2a**. The obtained crystal sample was, just in case, washed with a small amount of $CHCl_3$ and MeOH to remove the starting materials which might be slightly recrystallized. 6.68 mg, 76%. Calcd for $C_{56}H_{52}Mn_2N_4O_4Ni_2S_{20}$ (**2a**): C, 39.25; H, 3.06; N, 3.27. Found: C, 39.49; H, 3.03; N, 3.15. IR (KBr pellet, cm^{-1}): 1616, 1594, 1540, 1467, 1376, 1346, 1301, 1251, 1228, 1133, 1051, 1006, 819, 759, 736.

$[Mn(5\text{-Mesaltmen})\{Au(dmit)_2\}]_2$ (2b). To an acetone solution (4 mL) of $[Mn^{III}_2(5\text{-Mesaltmen})_2(H_2O)_2](PF_6)_2$ (3.30 mg, 0.00295 mmol) was added an acetone solution (4 mL) of $(NBu_4)[Au(dmit)_2]$ (4.46 mg, 0.0054 mmol), and then, the mixture was stirred for several minutes at room temperature to produce a brown solution. After 4 mL of toluene was added, this solution was divided into two portions and was kept, undisturbed, for 1 day at room temperature to yield black block-shaped crystals of **2b**. The obtained crystal sample was, just in case, washed with a small amount of $CHCl_3$ and MeOH to remove the starting materials which might be slightly recrystallized. 4.69 mg, 0.0024 mmol, 87%. Calcd for $C_{56}H_{52}Mn_2N_4O_4Au_2S_{20}$ (**2b**): C, 33.80; H, 2.63; N, 2.82. Found: C, 33.68; H, 2.88; N, 2.66. IR (KBr pellet, cm^{-1}): 1612, 1594, 1541, 1473, 1446, 1376, 1302, 1275, 1228, 1134, 1047, 1010, 906, 825, 759.

Physical Measurements. Infrared spectra were measured on KBr disks with a Jasco FT-IR 620 spectrophotometer. Magnetic susceptibility measurements were conducted with a Quantum Design SQUID magnetometer (MPMS-XL) in the temperature and direct current (dc) field ranges of 1.8−300 K and −7 to 7 T, respectively. Alternating current (ac) measurements were performed at various frequencies ranging from 1 to 1488 Hz with an ac field amplitude of 3 Oe. Polycrystalline samples embedded in liquid paraffin were measured. Experimental data were corrected for the sample holder, including the liquid paraffin, and for the diamagnetic contribution calculated from Pascal constants.[20] Magnetizations on field-aligned polycrystalline samples of **1a**, **1b**, and **2b** at 500 mK were measured with a ^{3}He refrigerator (IQUANTUM iHelium3) attached to the Quantum Design SQUID magnetometer MPMS-XL with application of up to ±1 T external field. The temperature dependence of susceptibility on polycrystalline samples of **1a**, **1b**, and **2b** below 1.8 K was also measured at 0.1 T using the same apparatus. Electrical conductivity of single crystals of **1a**, **1b**, **2a**, and **2b** was first checked with the two-probe method at room temperature using a common tester. The temperature dependence of two-probe dc resistance of single crystals of **1a** and **2a** was measured with current flow along the *a* axis of the crystal in the temperature range of 50−300 K using a Quantum Design PPMS. Electrical contacts to the crystal were made with 15 μm platinum wire and carbon paste. Crystal lattice orientation of the used single crystals of **1a**, **1b**, **2a**, and **2b** were first determined by X-ray crystallography using a CCD diffractometer (Bruker SMART), and the crystal ($0.2 \times 0.15 \times 0.05$ mm^3 for **1a**, $0.2 \times 0.2 \times 0.2$ mm^3 for **1b**, $0.45 \times 0.1 \times 0.1$ mm^3 for **2a**, $0.2 \times 0.2 \times 0.2$ mm^3 for **2b**) was used for the conductivity measurements.

Crystallography. Single crystals with dimensions of $0.3 \times 0.3 \times 0.2$ mm^3 for **1a**, $0.2 \times 0.2 \times 0.2$ mm^3 for **1b**, $0.55 \times 0.3 \times 0.3$ mm^3 for **2a**, and $0.2 \times 0.2 \times 0.2$ mm^3 for **2b** were mounted on a glass rod. Data collections were made on a Bruker SMART CCD diffractometer with a graphite monochromated Mo Kα radiation ($\lambda = 0.71070$ Å). Integrated intensities were obtained with SAINT+, and SADABS was used for absorption correction. The structures were solved by a direct method (SHELXS-97),[21] refined by full-matrix least-squares on F^2 (SHELXL-97)[21] on the basis of observed reflections and variable parameters, and converged with unweighted and weighted agreement factors of $R1 = \Sigma||F_o| - |F_c||/\Sigma|F_o|$ ($I > 2.00\sigma(I)$) and $wR2 = [\Sigma w(F_o^2 - F_c^2)^2/\Sigma w(F_o^2)^2]^{1/2}$ (all data). The non-

(16) (a) Kobayashi, A.; Fujiwara, E.; Kobayashi, H. *Chem. Rev.* **2004**, *104*, 5243. (b) Tanaka, H.; Okano, Y.; Kobayashi, H.; Suzuki, W.; Kobayashi, A. *Science* **2001**, *291*, 285.
(17) Miyasaka, H.; Clérac, R.; Ishii, T.; Chang, H.-C.; Kitagawa, S.; Yamashita, M. *J. Chem. Soc., Dalton Trans.* **2002**, 1528.
(18) Steimeche, G.; Sieler, H. J.; Kirmse, R.; Hoyer, E. *Phosphorus Sulfur Relat. Elem.* **1979**, *7*, 49.
(19) Matsubayashi, M.; Takahashi, K.; Tanaka, T. *J. Chem. Soc., Dalton Trans.* **1988**, 967.
(20) Boudreaux, E. A.; Mulay, L. N. *Theory and Applications of Molecular Paramagnetism*; John Wiley and Sons: New York, 1976; p 491.
(21) *SHELXTL-PC Package*; Bruker, AXS Inc.: Madison, WI, 1998.

Table 1. Crystallographic Data for **1a**, **1b**, **2a**, and **2b**

	1a	1b	2a	2b
formula	$C_{56}H_{52}Mn_2N_4Ni_2O_8S_{20}$	$C_{56}H_{52}Au_2Mn_2N_4O_8S_{20}$	$C_{56}H_{52}Mn_2N_4Ni_2O_4S_{20}$	$C_{56}H_{52}Au_2Mn_2N_4O_4S_{20}$
fw	1777.52	2054.03	1713.52	1990.02
crystal system	triclinic	triclinic	triclinic	triclinic
space group	$P\bar{1}$ (No. 2)	$P\bar{1}$ (No. 2)	$P\bar{1}$ (No. 2)	$P\bar{1}$ (No. 2)
λ (Mo Kα), Å	0.71073	0.71073	0.71073	0.71073
a, Å	8.671(2)	8.6523(12)	8.6580(8)	8.7142(11)
b, Å	13.178(3)	13.2808(18)	13.1671(11)	13.1811(15)
c, Å	15.701(4)	15.820(2)	15.1286(13)	15.1939(19)
α, deg	75.125(6)	76.034(3)	74.047(2)	73.934(3)
β, deg	74.769(5)	75.391(4)	78.740(2)	78.494(3)
γ, deg	79.107(6)	80.196(4)	78.576(2)	78.060(3)
V, Å^3	1658.8(7)	1695.5(4)	1607.2(2)	1621.9(3)
Z	1	1	1	1
T, K	100(2)	120(2)	120(2)	100(2)
μ (Mo Kα), cm^{-1}	1.618	5.349	1.662	5.584
D_{calcd}, g·cm^{-3}	1.779	2.012	1.770	2.037
F_{000}	906	1008	874	976
$2\theta_{max}$, deg	55	55	55	55
reflns msrd	16825	19799	16953	19591
reflns used	7597 (R_{int} = 0.0361)	9716 (R_{int} = 0.0270)	7380 (R_{int} = 0.0362)	9355 (R_{int} = 0.0371)
params.	421	421	403	403
$R1$, $wR2$ [$I > 2\sigma(I)$][a]	0.0434, 0.0813	0.0331, 0.0687	0.0373, 0.0750	0.0374, 0.0517
$R1$, $wR2$ [all data][b]	0.0697, 0.1008	0.0436, 0.0816	0.0574, 0.0953	0.0558, 0.0540
GOF on F^2	0.987	0.930	0.960	0.803
ρ_{max}/ρ_{min}, e$^-$·Å^{-3}	0.7380, 0.6425	0.4143, 0.4143	0.6355, 0.4618	0.4014, 0.4014

[a] $R1 = \Sigma||F_o| - |F_c||/\Sigma|F_o|$. [b] $wR2 = [\Sigma w(F_o^2 - F_c^2)^2/\Sigma w(F_o^2)^2]^{1/2}$.

Scheme 1

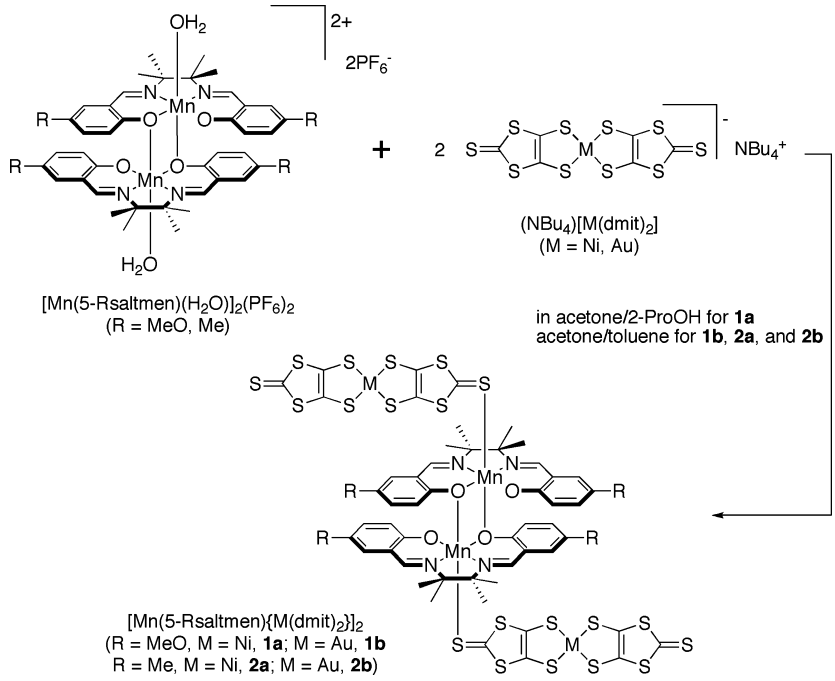

hydrogen atoms were refined anisotropically. Hydrogen atoms were refined using the riding model. The details of crystallographic data for **1a**, **1b**, **2a**, and **2b** are listed in Table 1.

CCDC-701627 for **1a**, CCDC-701628 for **1b**, CCDC-701629 for **2a**, and CCDC-701630 for **2b** contain the supplementary crystallographic data for this paper. These data can be obtained free of charge from The Cambridge Crystallographic Data Centre via www.ccdc.cam.ac.uk/data_request/cif.

Results and Discussion

Syntheses and Characterizations. Compounds **1a** and **2a** were synthesized by the reaction of $[Mn^{III}_2(5\text{-MeOsaltmen})_2(H_2O)_2](PF_6)_2$ or $[Mn^{III}_2(5\text{-Mesaltmen})_2(H_2O)_2](PF_6)_2$ with $(NBu_4)[Ni(dmit)_2]$ in a 1:2 mixing ratio (Mn:Ni = 1:1) in an acetone/2-propanol or toluene solution, respectively (Scheme 1). The same reactions employing $(NBu_4)[Au(dmit)_2]$ instead of $(NBu_4)[Ni(dmit)_2]$ were also performed for the purpose of synthesizing respective isostructural compounds, **1b** and **2b**, with a diamagnetic Au(III) ion. Note that the electrochemical reaction in solution containing the $[Mn^{III}_2(5\text{-MeOsaltmen})_2(H_2O)_2](PF_6)_2$ and $(NBu_4)[Ni(dmit)_2]$ precursors under anaerobic conditions has yielded a $[Mn_2]$:$[Ni(dmit)_2]$ = 1:7 stoichiometry in the $[Mn_2(5\text{-MeOsalt-}$

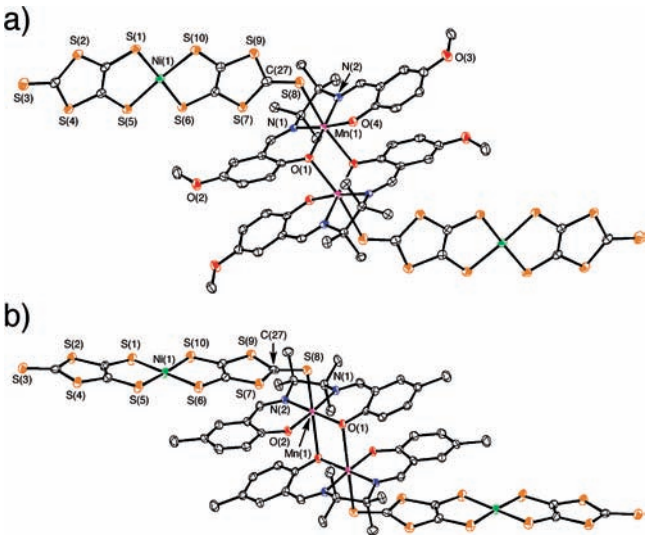

Figure 1. ORTEP views of **1a** and **2a** with atomic numbering schemes for selected atoms (50% probability thermal level).

men)$_2$(solv)$_2$][Ni(dmit)$_2$]$_7$·4(solv) (solv = acetone or acetonitrile, dependent on used solvent) compound reported previously.[15] Here, the crystallization was simply carried out by a solvent evaporation of reaction solutions under aerobic conditions. According to the stoichiometry of the mixing ratio, all compounds crystallize in a [Mn$_2$]:[M(dmit)$_2$] = 1:2 stoichiometric form leading to neutral single-component assemblies. The crystals of all compounds are very stable because of their solvent-free forms.

As expected from the formula and proved by the IR spectroscopy, the [M(dmit)$_2$]$^-$ unit is a monoanion in the whole series of materials. The vibration modes of $\nu_{C=C}$ and ν_{C-S} are very sensitive to the oxidation state of the [M(dmit)$_2$]$^{n-}$ unit[22−24] with [M(dmit)$_2$]$^{2-}$, about 1434 cm^{-1} and 1050 cm^{-1}; [M(dmit)$_2$]$^{1-}$, 1349 cm^{-1} and 1060 cm^{-1} with sharp bands; and noninteger-oxidized salts of [M(dmit)$_2$]$^{n-}$ ($1 > n > 0$; noninteger), 1260 cm^{-1} and 1062 cm^{-1} as broad bands for $\nu_{C=C}$ and ν_{C-S}, respectively. All present compounds show sharp bands in the range of 1348−1376 cm^{-1} for $\nu_{C=C}$ and 1047−1068 cm^{-1} for ν_{C-S}, proving the presence of the monoanionic [M(dmit)$_2$]$^-$ moiety. Interestingly, only **1a** and **2a** show a weak charge-transfer band in the wide range of 1600−4000 cm^{-1}, suggesting a conducting behavior (see below).

Structures. All compounds crystallize in the triclinic $P\bar{1}$ (No. 2) space group with the inversion center located at the midpoint of the Mn···Mn vector ($Z = 1$). The structures of the sets **1a/1b** and **2a/2b** are respectively isomorphous with a very similar structural building unit. Oak Ridge thermal ellipsoid plot (ORTEP) drawings of the asymmetrical units of **1a** and **2a** are depicted in Figure 1 (those of **1b** and **2b** are given in Figure S1 of Supporting Information), and relevant bond distances and angles of the sets **1a/1b** and **2a/2b** are listed in Tables 2 and 3, respectively. All compounds have an out-of-plane [Mn$^{III}_2$(5-Rsaltmen)$_2$]$^{2+}$ dinuclear core capped in apical positions by one of 2-thioketone sulfur atoms of [M(dmit)$_2$]$^-$ anion, forming a linear-type assembly of [(dmit)−M−(dmit)−Mn−(O$_{Ph}$)$_2$−Mn−(dmit)−M−(dmit)], where −(O$_{Ph}$)$_2$− is the biphenolate bridge of the out-of-plane dimer. The hexacoordinated Mn^{III} ion has an apically distorted octahedral geometry with a Jahn−Teller elongation axis of [S(8)−Mn(1)−O$_{Ph}$(1^a)] with Mn(1)−S(8) = 2.9936 (12) Å for **1a**, 2.9978 (12) Å for **1b**, 2.7172(10) Å for **2a**, and 2.7257(12) Å for **2b**; Mn(1)−O(1^a) = 2.389(2) Å for **1a**, 2.395(3) Å for **1b**, 2.557(2) Å for **2a**, and 2.501(3) Å for **2b**; and S(8)−Mn(1)−O(1^a) = 163.21(7)° for **1a**, 163.39(8)° for **1b**, 163.96(5)° for **2a**, and 163.68(6)° for **2b**. On the basis of this coordination sphere geometry, the Mn ions (Mn(1) and Mn(1^a)) are clearly trivalent. The Jahn−Teller axes at Mn(1) and Mn(1^a) are parallel to each other because of the existence of an inversion center located at the midpoint of the out-of-plane dimer (see above). The most important structural difference between the sets **1a/1b** and **2a/2b** is found in the dihedral angle made by the coordinating dmit plane defined by S(7)−S(8)−S(9)−C(27) and the Mn(saltmen) plane defined by O(1)−O(2)−N(2)−N(1)−Mn(1): 88.87(6)° and 88.46(11)° for **1a** and **1b**, respectively, and 14.84(15)° and 14.23(11)° for **2a** and **2b**, respectively. The bond angle of Mn(1)−S(8)−C(27) is 126.97(15)° and 127.78(15)° for **1a** and **1b**, respectively, and 103.01(11)° and 101.98(12)° for **2a** and **2b**, respectively, which also reveals

Table 2. Relevant Bond Distances (Å) and Angles (deg) for **1a**, **1b, 2a**, and **2b**

[Mn$_2$(5-MeOsaltmen)$_2$]$^{2+}$ Unit in **1a** and **1b**		
	1a	**1b**
Mn(1)−O(1)	1.905(2)	1.907(3)
Mn(1)−O(4)	1.850(2)	1.856(3)
Mn(1)−O(1)^a	2.389(2)	2.395(3)
Mn(1)−N(1)	1.975(3)	1.982(3)
Mn(1)−N(2)	1.969(2)	1.978(3)
Mn(1)−S(8)	2.9936(12)	2.9978(12)
S(8)−Mn(1)−O(1)	95.97(7)	96.18(7)
S(8)−Mn(1)−O(4)	79.00(7)	79.52(8)
S(8)−Mn(1)−O(1)^a	163.21(7)	163.39(8)
S(8)−Mn(1)−N(1)	96.29(8)	95.67(9)
S(8)−Mn(1)−N(2)	88.67(8)	88.26(9)
Mn(1)−S(8)−C(27)	126.97(15)	127.78(15)
Mn(1)−O(1)−Mn(1)^a	99.36(10)	99.03 (11)
O(1)−Mn(1)−O(1)^a	80.64(10)	80.97(11)
[Mn$_2$(5-Mesaltmen)$_2$]$^{2+}$ Unit in **2a** and **2b**		
	2a	**2b**
Mn(1)−O(1)	1.892(2)	1.902(2)
Mn(1)−O(2)	1.863(2)	1.868(3)
Mn(1)−O(1)^a	2.557(2)	2.501(3)
Mn(1)−N(1)	1.975(3)	1.985(3)
Mn(1)−N(2)	1.975(3)	1.973(3)
Mn(1)−S(8)	2.7172(10)	2.7257(12)
S(8)−Mn(1)−O(1)	89.16(7)	88.32(7)
S(8)−Mn(1)−O(2)	87.89(7)	87.40(7)
S(8)−Mn(1)−O(1)^a	163.96(5)	163.68(6)
S(8)−Mn(1)−N(1)	93.12(8)	92.41(7)
S(8)−Mn(1)−N(2)	98.33(8)	99.01(8)
Mn(1)−S(8)−C(27)	103.01(11)	101.98(12)
Mn(1)−O(1)−Mn(1)^a	99.06(9)	100.06(10)
O(1)−Mn(1)−O(1)^a	80.94(8)	79.94(10)

^{a} Symmetry operations: $2 - x$, $1 - y$, $-z$.

(22) Johnson, M. K. *Prog. Inorg. Chem.* **2004**, *52*, 213.
(23) (a) Zinenko, T. N.; Starodub, V. A.; Kazachkov, A. R. *Russ. J. Coord. Chem.* **2003**, *29*, 400. (b) Liu, G.; Fang, Q.; Xu, W.; Chen, H.; Wang, C. *Spectrochim. Acta, Part A* **2004**, *60*, 541.
(24) Pokhodnya, K. I.; Faulmann, C.; Malfant, I.; Andreu-Solano, R.; Cassoux, P.; Mlayah, A.; Smirnov, D.; Leotin, J. *Synth. Met.* **1999**, *103*, 2016.

Table 3. Relevant Bond Distances (Å) for **1a**, **1b, 2a**, and **2b**

[Ni(dmit)$_2$] in **1a**		[Ni(dmit)$_2$] in **2a**	
Ni(1)−S(1)	2.1644(11)	Ni(1)−S(1)	2.1512(10)
Ni(1)−S(5)	2.1587(12)	Ni(1)−S(5)	2.1591(10)
Ni(1)−S(6)	2.1613(11)	Ni(1)−S(6)	2.1704(10)
Ni(1)-S(10)	2.1783(12)	Ni(1)−S(10)	2.1602(10)
S(1)−C(23)	1.706(4)	S(1)−C(23)	1.711(3)
S(5)−C(25)	1.710(3)	S(5)−C(25)	1.710(3)
S(6)−C(26)	1.726(4)	S(6)−C(26)	1.715(3)
S(10)−C(28)	1.729(3)	S(10)−C(28)	1.718(3)
C(23)−C(25)	1.370(5)	C(23)−C(25)	1.368(4)
C(26)−C(28)	1.351(5)	C(26)−C(28)	1.368(4)
S(2)−C(23)	1.751(4)	S(2)−C(23)	1.742(3)
S(4)−C(25)	1.743(4)	S(4)−C(25)	1.734(3)
S(7)−C(26)	1.738(4)	S(7)−C(26)	1.738(3)
S(9)−C(28)	1.750(4)	S(9)−C(28)	1.727(3)
S(2)−C(24)	1.739(4)	S(2)−C(24)	1.731(3)
S(3)−C(24)	1.633(4)	S(3)−C(24)	1.645(4)
S(4)−C(24)	1.736(4)	S(4)−C(24)	1.734(3)
S(7)−C(27)	1.712(4)	S(7)−C(27)	1.717(3)
S(8)−C(27)	1.663(4)	S(8)−C(27)	1.677(4)
S(9)−C(27)	1.734(4)	S(9)−C(27)	1.715(3)
[Au(dmit)$_2$] in **1b**		[Au(dmit)$_2$] in **2b**	
Au(1)−S(1)	2.3304(10)	Au(1)−S(1)	2.3060(10)
Au(1)−S(5)	2.3189(12)	Au(1)−S(5)	2.3154(11)
Au(1)−S(6)	2.3264(11)	Au(1)−S(6)	2.3292(11)
Au(1)−S(10)	2.3388(12)	Au(1)−S(10)	2.3165(11)
S(1)−C(23)	1.753(5)	S(1)−C(23)	1.745(4)
S(5)−C(25)	1.755(4)	S(5)−C(25)	1.752(4)
S(6)−C(26)	1.750(4)	S(6)−C(26)	1.739(4)
S(10)−C(28)	1.754(4)	S(10)−C(28)	1.744(5)
C(23)−C(25)	1.339(6)	C(23)−C(25)	1.325(5)
C(26)−C(28)	1.342(6)	C(26)−C(28)	1.343(5)
S(2)−C(23)	1.757(4)	S(2)−C(23)	1.751(4)
S(4)−C(25)	1.747(5)	S(4)−C(25)	1.754(4)
S(7)−C(26)	1.738(4)	S(7)−C(26)	1.746(4)
S(9)−C(28)	1.763(5)	S(9)−C(28)	1.733(4)
S(2)−C(24)	1.746(5)	S(2)−C(24)	1.732(4)
S(3)−C(24)	1.640(5)	S(3)−C(24)	1.642(4)
S(4)−C(24)	1.728(5)	S(4)−C(24)	1.733(4)
S(7)−C(27)	1.721(5)	S(7)−C(27)	1.723(3)
S(8)−C(27)	1.666(4)	S(8)−C(27)	1.670(4)
S(9)−C(27)	1.734(4)	S(9)−C(27)	1.713(4)

a large difference between the structures of the sets **1a** and **1b**and **2a** and **2b**.

Packing Feature. The present single-component materials made of [Mn(5-Rsaltmen){M(dmit)$_2$}]$_2$ complexes display strong intermolecular interactions formed by $\pi-\pi$ and S···S contacts from both dinuclear Mn core and [M(dmit)$_2$]$^-$ moieties. A true segregation is observed with two kinds of layers (Figure 2 shows the packing features of **1a** and **2a**, those of **1b** and **2b** being essentially identical to them, respectively). The [Mn$_2$(5-Rsaltmen)$_2$] moieties arranged in the *a* axis direction make weak C···C, C···O, and O···O contacts in the phenyl ring and 5-R substituent of the 5-Rsaltmen ligand (C···O ≈ 3.1 Å for **1a** and **1b** and C···C ≈ 3.4 Å for **2a** and **2b**; Figure S2 of Supporting Information). The most important contacts are seen between [M(dmit)$_2$]$^-$ moieties that stack and form stair-like zigzag columns along the *a* axis direction (Figures 2 and 3). These columns are composed of face-to-face $\pi-\pi$ and S···S interactions (M···M distance: 4.129 Å for **1a**, 4.164 Å for **1b**, 4.256 Å for **2a**, 4.238 Å for **2b**) and side-by-side S···S interactions (M···M distance: 6.433 Å for **1a**, 6.422 Å for **1b,** 7.384 Å for **2a**, 7.512 Å for **2b**) between adjacent [M(dmit)$_2$]$^-$ molecules. The relevant S···S contacts are listed in Table 4. In both interacting modes, the shortest one is found in the range of 3.5−3.7 Å for **1a** and **1b** and 3.6−3.7 Å for **2a** and **2b** (see Table 4).

Electrical Conductivity. The electrical dc conductivity on single crystals of all compounds was first measured at room temperature (using a two-probes method). While for **1b** and **2b** the conductivity, σ, was at less than 10^{-6} S·cm^{-1} (insulator) at room temperature, **1a** and **2a** yielded the measurable conductivity as $\sigma = 7 \times 10^{-4}$ S·cm^{-1} and 1×10^{-4} S·cm^{-1} at 300 K, respectively. Therefore, the temperature dependence of σ was measured for **1a** and **2a** between 300 and 50 K. As expected from the IR data and the packing structure, these compounds show a measurable transport property when the probes are attached in the direction of the [M(dmit)$_2$]$^-$ stair-like column (the *a* axis direction). The conductivity of **1a** and **2a** in this direction decreases gradually with decreasing temperature and becomes too small to be measured by our technique at approximately 150 and 220 K, respectively. This temperature dependence of **1a** and **2a** reveals their semiconducting behavior with activation energies of 0.182 and 0.292 eV, respectively (Figure 4). Despite the integer valence of the [Ni(dmit)$_2$]$^-$ moiety, the observed conductivities are surprisingly large. Indeed, as far as we know, only one other compound is known with [Ni(dmit)$_2$]$^-$, the salt of *p*-EPYNN[Ni(dmit)$_2$] (*p*-EPYNN = *p*-*N*-ethylpyridinium α-nitronyl nitroxide), that displays a conductivity of 1.3×10^{-4} S·cm^{-1} at room temperature.[25]

Magnetic Contributions of [Ni(dmit)$_2$]$^-$ Moieties. The [Ni(dmit)$_2$]$^-$ complexes are associated into inversion-centered motifs, interacting with each other along the *a*-axis direction to form an alternated-chain motif. The overlap interaction energies (H_{ij}) associated with the HOMO···HOMO overlaps of the [Ni(dmit)$_2$]$^-$ moieties within (intra) and between (inter) the inversion centered dimeric motifs (H_{intra}, H_{inter}) were obtained from tight binding extended Hückel calculations.[26] These calculated interaction energies have proved to be very useful in discussing the electronic structures of many organic cation radical salts[27] and conducting[28] or paramagnetic[29] dithiolene complexes. They amount here to H_{intra}(**1a**) = 0.68 eV and H_{inter}(**1a**) = 0.043 eV for **1a** while slightly weaker values were obtained for **2a** with H_{intra}(**2a**) = 0.41 eV and H_{inter}(**2a**) = 0.028 eV. Other interactions through overlap of the outer C═S groups are negligible. As a consequence of the very large $H_{\text{intra}}/H_{\text{inter}}$ ratio in both salts, one expects a simple singlet−triplet state for the [Ni(dmit)$_2$]$^-$ rather than an alternated spin chain with a very weak magnetic contribution at room temperature, as a result of the strong dimerization of the [Ni(dmit)$_2$]$^-$ units. As the magnetic interaction

(25) Imai, H.; Otsuka, T.; Naito, T.; Awaga, K.; Inabe, T. *J. Am. Chem. Soc.* **1999**, *121*, 8098.
(26) (a) Whangbo, M.-H.; Hoffmann, R. *J. Am. Chem. Soc.* **1978**, *100*, 6093. (b) Ren, J.; Liang, W.; Whangbo, M.-H. *Crystal and Electronic Structure Analysis Using CAESAR*; 1998.
(27) Whangbo, M.-H.; Williams, J. M.; Leung, P. C. W.; Beno, M. A.; Emge, T. J.; Wang, H. H. *Inorg. Chem.* **1985**, *24*, 3500.
(28) (a) Canadell, E.; Ravy, S.; Pouget, J. P.; Brossard, L. *Solid State Commun.* **1990**, *75*, 633. (b) Whangbo, M. H.; Canadell, E.; Foury, P.; Pouget, J. P. *Science* **1991**, *252*, 96.
(29) (a) Fourmigué, M. *Acc. Chem. Res.* **2004**, *37*, 179. (b) Clérac, R.; Fourmigué, M.; Gaultier, J.; Barrans, Y.; Albouy, P.-A.; Coulon, C. *Eur. Phys. J. B* **1999**, *9*, 431.

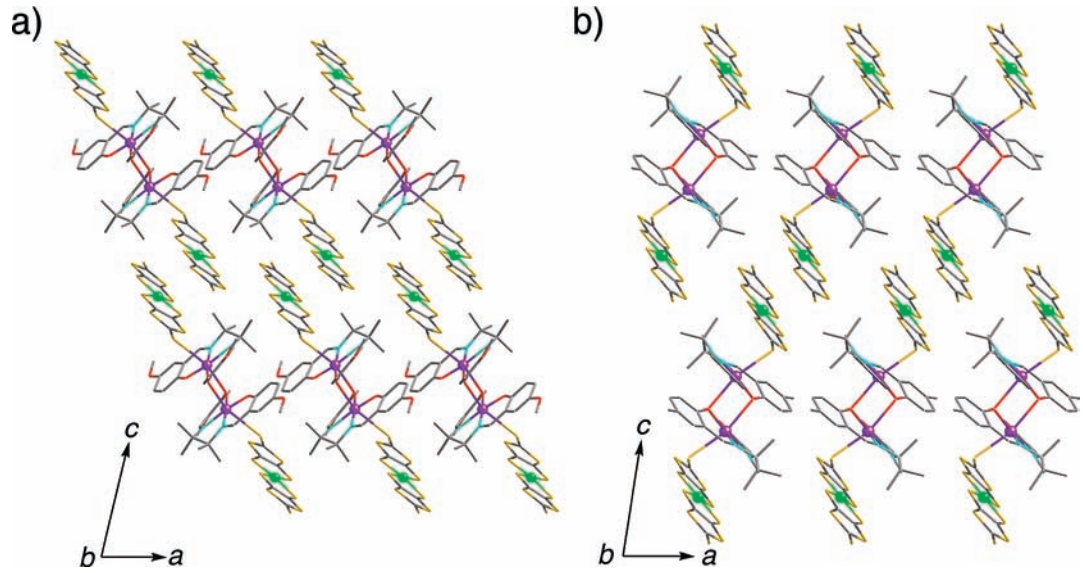

Figure 2. Packing arrangements of **1a** (a) and **2a** (b) projected along the *b* axis.

parameter, J_{Ni-Ni} is written as $(H_{ij})^2/U$, where U is the on-site Coulomb repulsion; one expects the J_{Ni-Ni}(**1a**)/J_{Ni-Ni}(**2a**) ratio to be close to $[H_{intra}(\mathbf{1a})/H_{intra}(\mathbf{2a})]^2$, that is, around 2.75.

dc Magnetic Properties. The magnetic susceptibility was measured on polycrystalline samples of **1a**, **1b**, **2a**, and **2b** at 0.1 T in the temperature range of 1.8−300 K (in field cooled mode) using a Quantum Design SQUID magnetometer MPMS-XL and in the range of 0.5−1.8 K (in zero-field cooled mode) using a ^{3}He refrigerator (IQUANTUM iHelium3) attached to the MPMS-XL SQUID magnetometer. The two types of measurement are well aligned, and no experimental discontinuity around 1.8 K is observed (Figure 5). The susceptibility obeys the Curie−Weiss law through the whole temperature range for **1a**, **1b**, and **2b** and above 20 K for **2a** with $C = 5.9$ cm^3·K·mol^{-1}, $\theta = +5.0$ K for **1a**; $C = 5.9$ cm^3·K·mol^{-1}, $\theta = +5$ K for **1b**; $C = 6.32$ cm^3·K·mol^{-1}, $\theta = -16$ K for **2a**; and $C = 5.8$ cm^3·K·mol^{-1}, $\theta = +5$ K for **2b**. The Curie constants are very similar to each other independently of the M^{III} metal ion (Ni^{III}, $S = 1/2$ or Au^{III}, $S = 0$) and very close to the expected spin-only value at 6.0 cm^3·mol^{-1} for two isolated $S = 2$ Mn(III) spins ($g = 2.00$). This result is consistent with the Hückel calculations that revealed a strong dimerization of $[Ni(dmit)_2]^-$ moieties leading to diamagnetic pairs.

Figure 5 displays χT versus T plots of **1a**, **1b**, **2a**, and **2b** at 0.1 T. The χT products of **1a** slightly decrease from 6.09 cm^3·K·mol^{-1} at 300 K to 6.03 cm^3·K·mol^{-1} at 185 K and then increase to 7.67 cm^3·K·mol^{-1} at 1.41 K followed by a decrease to 6.16 cm^3·K·mol^{-1} at 0.48 K. Although the slight decrease at high temperatures might be attributed to the contribution of the excited triplet spins of dimerized $[Ni^{III}(dmit)_2]^-$, the χT value at room temperature is consistent with the value expected from the spin-only value of two $S = 2$ excluding the diamagnetic pairs of $S = 1/2$ $[Ni^{III}(dmit)_2]^-$ units. As a confirmation, the global χT behaviors of **1a** and **1b** with $[Au^{III}(dmit)_2]^-$ ($S = 0$) are essentially identical: the χT products of **1b** slightly increase from 6.06 at 300 K to 8.06 cm^3·K·mol^{-1} at 1.6 K and then decrease to 6.36 cm^3·K·mol^{-1} at 0.47 K. Therefore, the magnetic behavior of **1a** as well as of **1b** should be only due to the contribution of Mn(III) dimer. To evaluate the intradimer magnetic coupling between Mn^{III} ions via a biphenolate bridge, the χT versus T plots of **1a** and **1b** were simulated by a Heisenberg $S = 2$ dimer model, taking into account the magnetic anisotropy arisen from each Mn(III) ion (zero-field splitting, D_{Mn}) and intermolecular interactions (zJ') introduced in the frame of the mean-field approximation ($H = -2J_{Mn-Mn}\vec{S}_{Mn1}\vec{S}_{Mn2} + 2D_{Mn}S_{Mn,z}^2$, where $S_{Mn,z}$ is the z component of the S_{Mni} spin vectors).[17,30,31] The best simulations for **1a** and **1b** were given as red lines in Figure 5, and the obtained parameter sets are $g = 2.01$, $J_{Mn-Mn}/k_B = +0.23$ K, $D_{Mn}/k_B = -0.71$ K, and $zJ'/k_B = -0.03$ K for **1a** and $g = 2.01$, $J_{Mn-Mn}/k_B = +0.31$ K, $D_{Mn}/k_B = -0.95$ K, and $zJ'/k_B = -0.02$ K for **1b**. These parameters are very similar to each other, but J_{Mn-Mn} and D_{Mn} are relatively smaller than those of related compounds previously reported.[17,30−34]

On the other hand, the temperature dependence of χT for **2a** is completely different from those of **1a** and **1b**. The χT product monotonically decreases from 5.68 cm^3·K·mol^{-1} at 300 K to 0.27 cm^3·K·mol^{-1} at 1.8 K. In addition, χ shows a maximum at 6.4 K followed by a decrease, suggesting the occurrence of a long-range antiferromagnetic order at this temperature (T_N; inset of Figure 5). As in **1a**, the χT value at 300 K suggests that the magnetic contribution of $[Ni^{III}(dmit)_2]^-$ units can be negligible, but it is not easy to judge if the main contribution for the antiferromagnetic coupling is coming from the Mn···Mn interaction via the biphenolate bridge or via the singlet $[Ni(dmit)_2]^-$ dimer. However, the magnetic behavior of **2b** is typical for ferromagnetically coupled Mn(III) dimers: the χT products slightly increase from 5.94 cm^3·K·mol^{-1} at 300 K to 7.90 cm^3·K·mol^{-1} at

(30) Miyasaka, H.; Clérac, R.; Wernsdorfer, W.; Lecren, L.; Bonhomme, C.; Sugiura, K.; Yamashita, M. *Angew. Chem., Int. Ed.* **2004**, *43*, 2801.
(31) Kachi-Terajima, C.; Miyasaka, H.; Saitoh, A.; Shirakawa, N.; Yamashita, M.; Clérac, R. *Inorg. Chem.* **2007**, *46*, 5861.
(32) Kachi-Terajima, C.; Miyasaka, H.; Sugiura, K.; Clérac, R.; Nojiri, H. *Inorg. Chem.* **2006**, *45*, 4381.
(33) Lü, Z.; Yuan, M.; Pan, F.; Gao, S.; Zhang, D.; Zhu, D. *Inorg. Chem.* **2006**, *45*, 3538.
(34) Miyasaka, H.; Saitoh, A.; Abe, S. *Coord. Chem. Rev.* **2007**, *251*, 2622.

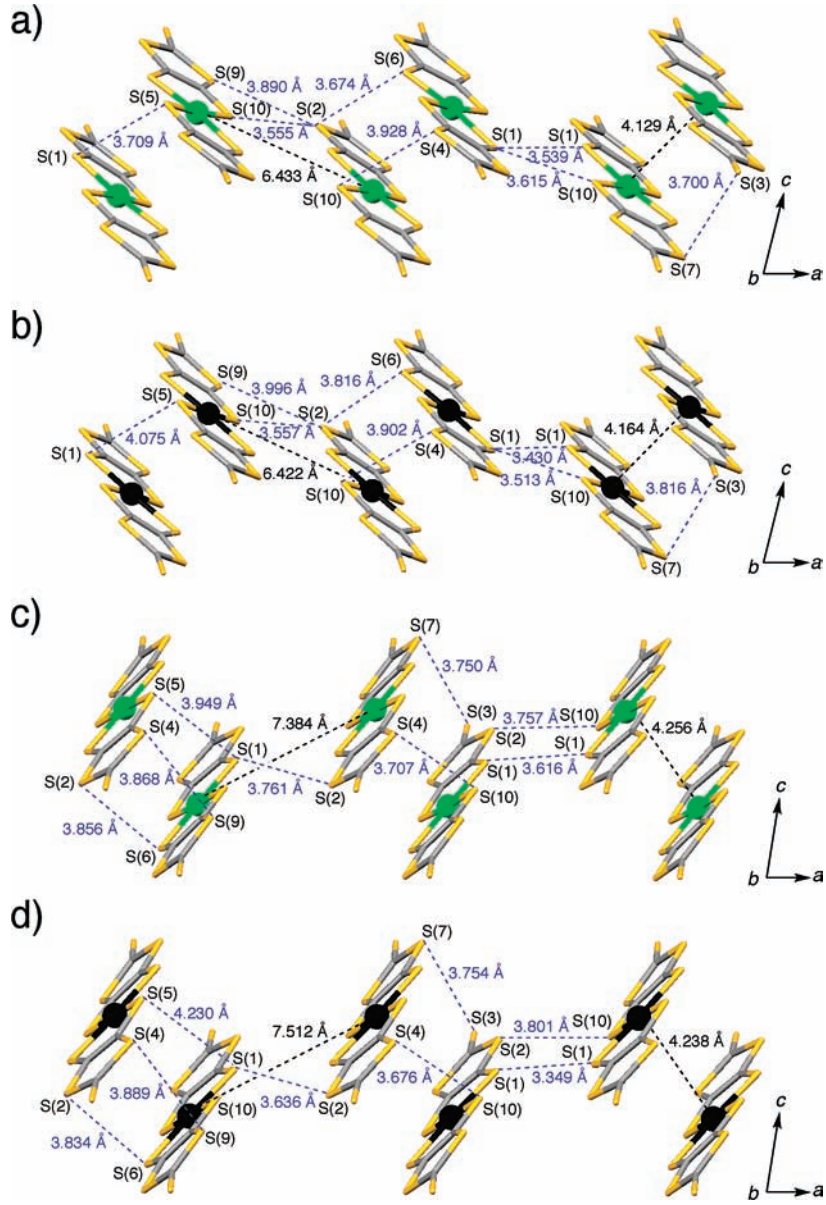

Figure 3. Short S···S contacts (blue dots) and M···M distances (black dots) in the stair-like stacking column of $[M(dmit)_2]^-$ moieties of **1a** (a), **1b** (b), **2a** (c), and **2b** (d).

Table 4. M···M and S···S Distances (Å) in the Stacking Arrangement of $[M(dmit)_2]^-$ Moieties

face-to-face			side-by-side		
contacts	**1a**	**1b**	contacts	**1a**	**1b**
M···M	4.129	4.164	M···M	6.433	6.422
S(1)···S(5)	3.709	4.075	S(1)···S(1)	3.539	3.430
S(2)···S(6)	3.674	3.816	S(1)···S(10)	3.615	3.513
S(3)···S(7)	3.700	3.816	S(2)···S(9)	3.890	3.996
S(4)···S(10)	3.928	3.902	S(2)···S(10)	3.555	3.557
face-to-face			side-by-side		
contacts	**2a**	**2b**	contacts	**2a**	**2b**
M···M	4.256	4.238	M···M	7.384	7.512
S(1)···S(5)	3.949	4.230	S(1)···S(1)	3.616	3.349
S(2)···S(6)	3.856	3.834	S(1)···S(2)	3.761	3.636
S(3)···S(7)	3.750	3.754	S(2)···S(10)	3.757	3.801
S(4)···S(9)	3.868	3.889			
S(4)···S(10)	3.707	3.676			

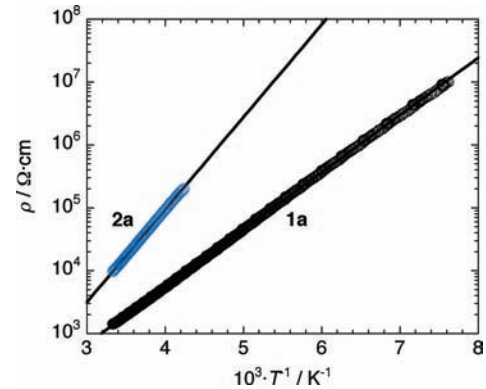

Figure 4. Temperature dependence of electrical resistivity on single crystals of **1a** and **2a** using a two-probe attachment along the stair-like $[Ni(dmit)_2]^-$ column.

3.43 K followed by a decrease to 5.30 $cm^3 \cdot K \cdot mol^{-1}$ at 0.46 K, essentially identical to those of **1a** and **1b**. The best set of parameters obtained fitting the experimental χT versus T data with the previously anisotropic Heisenberg $S = 2$ dimer model is $g = 1.99$, $J_{Mn-Mn}/k_B = +0.57$ K, $D_{Mn}/k_B = -1.91$

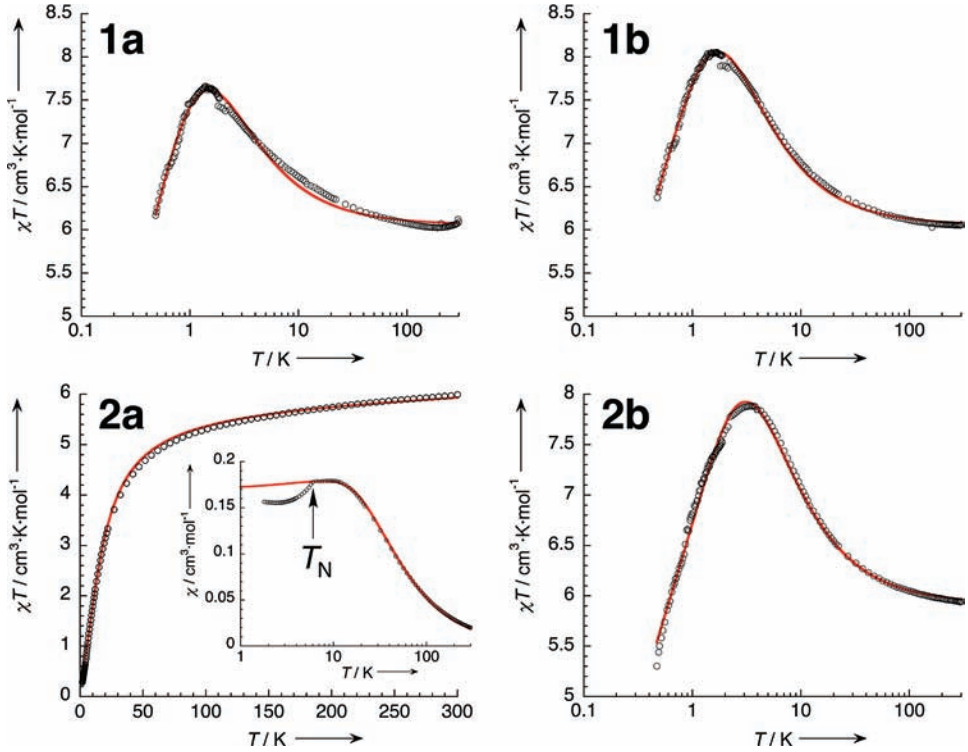

Figure 5. Temperature dependence of χT measured at 1 kOe for **1a**, **1b**, **2a**, and **2b**. Solid red lines represent the best fits obtained with the models described in the text.

K, and $zJ'/k_B = -0.03$ K for **2b**. Considering the isostructural packing of **2a** and **2b** and magnetic properties of **2b**, the dominant antiferromagnetic coupling in **2a** should be due to an exchange pathway through a singlet $[Ni^{III}(dmit)_2]^-$ pair (i.e., $\{Mn^{III}-[Ni^{III}(dmit)_2]\cdots[Ni^{III}(dmit)_2]-Mn^{III}\}$ path; see Figure 2). Indeed, on the basis of the crystal packing, chains of $\{Mn^{III}-[Ni^{III}(dmit)_2]\cdots[Ni^{III}(dmit)_2]-Mn^{III}\}$ units are formed as shown in Figure 2, neglecting the much weaker inter-$[Ni^{III}(dmit)_2]_2$ dimer exchange shown in Figure 3 (see also the Hückel calculations part). Therefore, to evaluate the effective exchange between Mn(III) ions via the singlet $[Ni^{III}(dmit)_2]_2^{2-}$ dimer, J_{eff}, the magnetic properties (χ versus T and χT versus T data) of **2a** were fitted to a Heisenberg chain model with classical $S = 2$ spins and two alternated magnetic interactions: J_{Mn-Mn} and J_{eff} (using the following Hamiltonian: $H = -2J_{eff}\sum_i \vec{S}_{2i}\vec{S}_{2i+1} - 2J_{Mn-Mn}\sum_i \vec{S}_{2i+1}\vec{S}_{2i+2}$. The analytical expression of the susceptibility derived from this model was reported by Cortés et al.,[35] who applied the Fisher approach.[36] It is worth noting that the effect of the magnetic anisotropy was neglected, as the data have been fitted only above 7 K in the paramagnetic phase. Using the full set of parameters (g, J_{Mn-Mn}, and J_{eff}) free leads to excellent fits of both χ versus T and χT versus T data, but multiple solutions were found as an indication of overparametrization of the model. Therefore, according the isostructural packing of **2a** and **2b**, J_{Mn-Mn}/k_B has been fixed at $+0.57$ K, found for **2b**. In this condition, the fits of both χ versus T and χT versus T data stay excellent as shown in Figure 5, with $g = 1.97$ and $J_{eff}/k_B = -2.85$ K. Despite a long distance between Mn^{III} spins, the exchange through the singlet $[Ni^{III}(dmit)_2]\cdots[Ni^{III}(dmit)_2]$ pair, J_{eff}, is surprisingly large. The origin of such a large exchange should be associated with the singlet−triplet excitation of the dimeric $[Ni^{III}(dmit)_2]^-$ moiety and might be similar to what is seen in a superexchange mechanism.

Magnetostructural Correlation. Despite a similar structural motif of **1a** and **2a**, their magnetic properties are completely different. Considering the similarity between **1a** and **2a**, this result can be easily attributed to different Mn(III)···Mn(III) interactions through $[Ni^{III}(dmit)_2]^-$ units that are effective in **2a** or not in **1a**. Indeed, to discuss this result, two important overlaps are relevant: (i) the one between $[Ni^{III}(dmit)_2]^-$ moieties and also (ii) those between the $[Ni^{III}(dmit)_2]^-$ group and the coordinating Mn(III) ion, especially the overlap between the HOMO on the terminal S (2-thioketone S) of $[Ni^{III}(dmit)_2]^-$ and the d_{z^2} orbital of Mn(III) ion (note that when Mn(III) ion has $^5B_{1g}$ ground-state with elongated Jahn−Teller distortion, four unpaired electrons are assigned as $d_{xy}^1d_{yz}^1d_{xz}^1d_{z^2}^1$, where the Jahn−Teller axis is parallel to the z axis[34]). According to molecular orbital calculations, the HOMO on the terminal S is made from one of the p orbitals,[16a] which aligns perpendicular to the dmit plane, so the overlap with the d_{z^2} orbital is strongly dependent on the angles of Mn−S−C and the dihedral angle between the dmit plane and the equatorial plane around the Mn ion. As mentioned in the structural section, huge geometrical differences are indeed observed on the **1a** and **2a** complex core. In particular, the small dihedral angle in **2a** (14.84°) should favor a strong σ-type overlap, which generally

(35) Cortés, R.; Drillon, M.; Solans, X.; Lezama, L.; Rojo, T. *Inorg. Chem.* **1997**, *36*, 677.
(36) Fisher, M. E. *Am. J. Phys.* **1974**, *32*, 241.

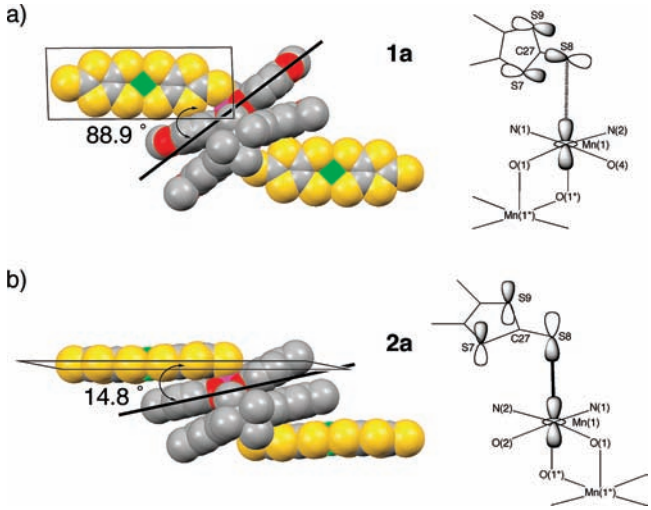

Figure 6. View of coordination modes between the $[Ni(dmit)_2]^-$ moiety and the Mn(III) metal ion in **1a** (a) and **2a** (b) (left), where the given angles are the dihedral angles between least-squares planes defined by S(7)−S(8)−S(9)−C(27) (for dmit) and O(1)−O(2)−N(2)−N(1)−Mn(1) (for Mn(saltmen)) and on the right, schematic orbital configurations of the d_{z^2} orbital of Mn ion and a p orbital of S(8) in **1a** (a) and **2a** (b).

contributes to antiferromagnetic coupling (Figure 6).[37] On the other hand, the large dihedral angle in **1a** (88.87°) should lead to a nonbonding situation (Figure 6) and thus very weak $Mn\cdots[Ni^{III}(dmit)_2]^-$ interactions. These structural differences are well in line with the magnetic behavior reported for **1a** and **2a** (Figure 5), especially considering that the overlaps between the $[Ni^{III}(dmit)_2]^-$ moieties described above are quite similar (Figures 2 and 3; see also the Hückel calculation part) and thus should not dramatically influence the observed properties.

ac Magnetic Properties and M versus H Behavior of Field-Oriented Crystals of 1a, 1b, and 2b. Compounds **1a**, **1b**, and **2b**, which are essentially ferromagnetic $[Mn^{III}_2(saltmen)_2]^{2+}$ dimers with an $S_T = 4$ ground state, are candidates to behave as SMMs as shown previously.[30,31,33] The temperature dependence of ac susceptibilities (10−1500 Hz) of these compounds was first measured at 3 Oe ac field and zero dc field. Both in-phase (χ') and out-of-phase (χ'') components are frequency dependent at low temperatures below 4 K (Figure S3, Supporting Information), but distinct peaks of χ'' were not observed above 1.8 K for all compounds (note that no ac signal was observed for **2a**, even around 6.4 K as expected for an antiferromagnetic order). To probe the thermally activated dynamics of these compounds, the same measurements were performed at 1.8 K under several dc fields (Figure 7), at which the QTM pathway of relaxation is expected to be at least partially suppressed by Zeeman effects that remove the degeneracy of the $\pm m_S$ state levels.[31,32,38,39] With increasing dc field, clear χ'' peaks are observed for **1a**, **1b**, and **2b** (Figure 7), and the characteristic dc field dependence of the relaxation time can

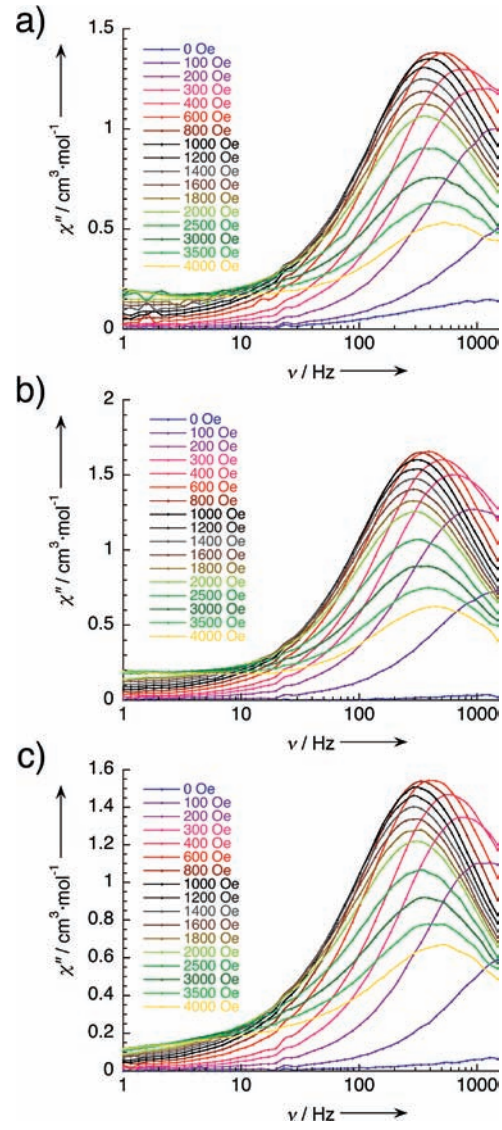

Figure 7. Frequency dependence of the out-of-phase component of ac susceptibility for **1a** (a), **1b** (b), and **2b** (c) at several applied dc fields at 1.8 K.

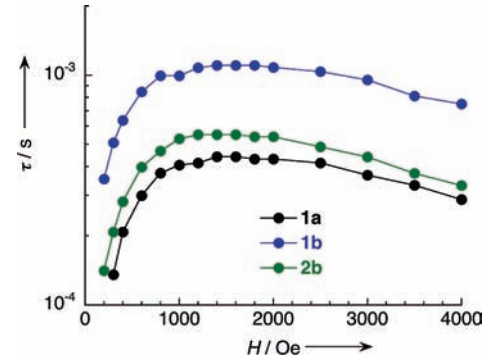

Figure 8. Field dependence of relaxation time (τ) at 1.8 K estimated from maximum of χ'' shown in Figure 7.

be plotted as shown in Figure 8. The maximum value was observed around 1500 Oe for **1a** and **1b** and 1200 Oe for **2b**, and τ_0 and Δ_{eff} at these fields were obtained as 8.2×10^{-7} s and 11.4 K for **1a**, 1.1×10^{-6} s and 12.5 K for **1b**, and 2.9×10^{-7} s and 13.6 K for **2b** by measuring temperature dependence of ac susceptibility (Figure S4, Supporting

(37) Kahn, O. *Molecular Magnetism*; VCH Publishers, Inc.: Weinheim, Germany, 1993.
(38) Thomos, L.; Lionti, F.; Ballou, R.; Gatteschi, D.; Sessoli, R.; Barbara, B. *Nature* **1996**, *383*, 145.
(39) Ako, A. M.; Mereacre, V.; Hewitt, I. J.; Clérac, R.; Lecren, L.; Anson, C. E.; Powell, A. K. *J. Mater. Chem.* **2006**, *16*, 2579.

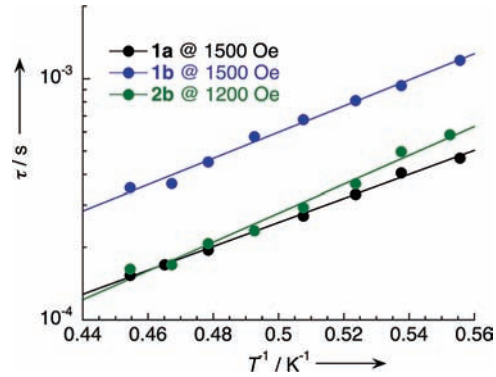

Figure 9. Arrhenius plots of the relaxation times measured at 1500 Oe for **1a** and **1b** and 1200 Oe for **2b**.

Information) and making Arrhenius plots as shown in Figure 9. These behaviors prove that **1a**, **1b**, and **2b** exhibit typical SMM behavior. To obtain further information on SMM behavior, the field dependence of the magnetization was measured on field-oriented single crystals at 500 mK with a 2 Oe/s sweep rate (Figure 10). Only a small butterfly-type hysteresis was observed in **2b**, while a simple monotonic sigmoidal magnetization was observed in **1a** and **1b**. This behavior is consistent with a fast zero-field quantum tunneling and the small energy barrier of the magnetization in these compounds induced by the small magnetic anisotropy of the ground-state that is characterized by a D_{ST} parameter of less than 1.0 K.

Conclusion

The aerobic reaction of $[Mn_2(5\text{-Rsaltmen})_2(H_2O)_2](PF_6)_2$ (R = MeO, Me) with $(NBu_4)[M(dmit)_2]$ (M = Ni, Au) in a 1:2 molar ratio (Mn:M = 1:1) in acetone/2-propanol or toluene yielded stoichiometric neutral assemblies with a formula of $[Mn(5\text{-Rsaltmen})\{M(dmit)_2\}]_2$ (R = MeO, M = Ni, **1a**; M = Au, **1b**; R = Me, M = Ni, **2a**; M = Au, **2b**) by a simple ion exchange removing $(NBu_4)PF_6$. These compounds are Mn(III) saltmen out-of-plane dimers decorated by $[M(dmit)_2]^-$ in apical positions, forming a linear-type tetranuclear complex, [M−(dmit)−Mn−$(O_{Ph})_2$−Mn−(dmit)−M]. The Mn ions are trivalent from the structural characteristics, and the $[M(dmit)_2]^-$ unit is consequently monovalent. Despite such a simple assembly composed of a single-component,[16] that is, single neutral complex, **1a** and **2a**, the Ni analogues (M = Ni) behave as semiconductors with $\sigma_{r.t.} = 7 \times 10^{-4}$ S·cm^{-1} and $E_a = 182$ meV for **1a** and $\sigma_{r.t.} = 1 \times 10^{-4}$ S·cm^{-1} and $E_a = 292$ meV for **2a** ($\sigma_{r.t.}$ is the conductivity at room temperature and E_a is activation energy between the valence band and the conducting band), while **1b** and **2b** with M = Au are insulators. This conductivity results from the 1D columnar arrangement of $[Ni(dmit)_2]^-$ moieties with $\pi-\pi$ and S···S contacts along the *a* axis direction. Nevertheless, the obtained electrical conductivity values of about 10^{-4} S·cm^{-1} stay weak because of the absence of mixed valence and the presence of a strong dimerization along the $[Ni(dmit)_2]^-$ columns. Indeed, Hückel calculations confirm the strong intermolecular dimerization in $[Ni(dmit)_2]^-$ columns leading to singlet $[Ni(dmit)_2]^-$ pairs.

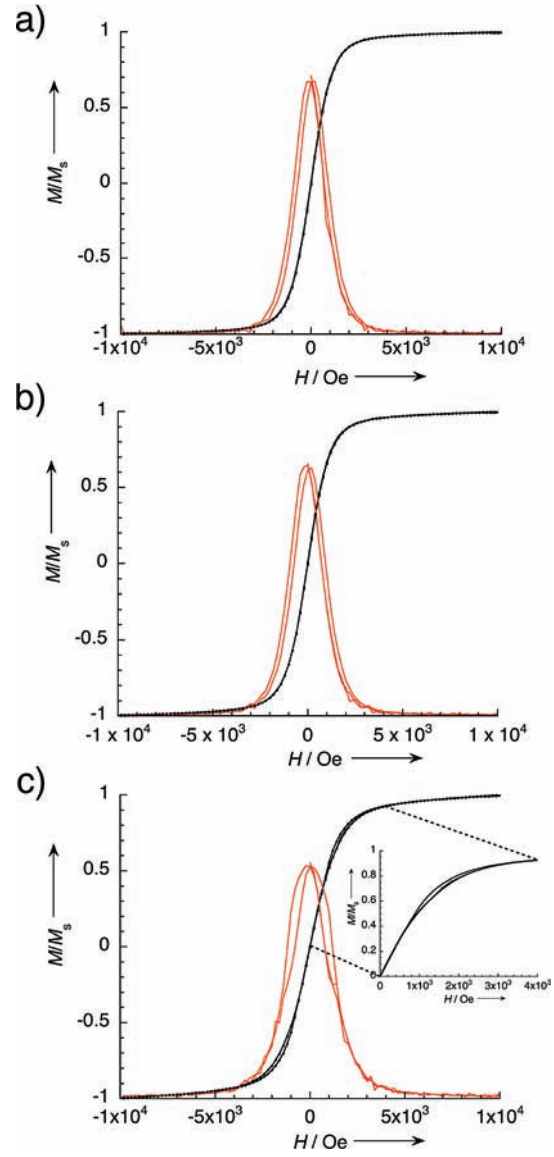

Figure 10. Field dependence of magnetization measured on field-oriented single crystals of **1a** (a), **1b** (b), and **2b** (c) at 500 mK with a 2 Oe/s sweep rate. Red lines represent d*M*/d*H* versus *H* plot (arbitrary scale). Inset of part c: zoom of the *M* versus *H* plot for **2b**, emphasizing the hysteresis effect.

Thus, the $[Ni(dmit)_2]^-$ spins stay silent below 300 K, and the magnetic properties of **1a** are essentially identical to those of **1b** and **2b**. These compounds exhibit SMM properties with slow magnetization relaxation at low temperatures and fast zero-field QTM. On the other hand, the magnetic properties of **2a** are dominated by the intercomplex Mn···Mn antiferromagnetic interactions ($J_{eff}/k_B = -2.85$ K) via the singlet $[Ni(dmit)_2]^-$ dimer that stabilize a long-range antiferromagnetic order at $T_N = 6.4$ K. The relatively strong antiferromagnetic interactions via this singlet pair (despite a long Mn−Mn distance) are probably associated with the singlet−triplet excitation of the dimeric $[Ni^{III}(dmit)_2]^-$ moiety and might be similar to what is seen in a superexchange mechanism. The magnitude of this intermolecular Mn···Mn interaction is indeed mainly dependent on the Mn/$[Ni(dmit)_2]^-$ orbital orientations and the strength of the σ-type orbital overlap on the Mn−S bond.

The present compounds that display multiple properties, semiconductor/SMM for **1a**, insulator/SMM for **1b** and **2b**, and semiconductor/antiferromagnet for **2a**, are indeed rare examples of materials made of neutral single-component molecules exhibiting two major solid-state properties such as electrical conductivity and magnetism. The important aspect in the present materials is that the bonding between the magnetic-contributing part and the conductive-contributing part tuned their magnetic properties without significant changing of electrical properties, as seen in **1a** and **2a**. These materials illustrate a new synthetic approach toward the design of polyfunctional (magnetic-conducting) materials that display synergic properties.[40] The impact of such materials will open intriguing perspectives in the fields of molecular electronics and devices.

Acknowledgment. We thank Prof. C. Coulon (CRPP, Bordeaux, France) for stimulating discussions that helped us to improve the physical interpretation of our magnetic data. This work was financially supported by the CREST project, Japan Science and Technology Agency (JST); a Grant-in-Aid for Scientific Research (Grant No. 18685007) from the Ministry of Education, Culture, Sports, Science, and Technology, Japan (H.M.); the University of Bordeaux (R.C.); The University of Rennes 1 (M.F.); and the CNRS and the "Région Aquitaine" (R.C. and M.F.).

Supporting Information Available: X-ray crystallographic files in CIF format for **1a**, **1b**, **2a**, and **2b** and additional structural magnetic data of Figures S1−S4. This material is available free of charge via the Internet at http://pubs.acs.org.

IC802110B

(40) Matsushita, M. M.; Kawakami, H.; Sugawara, T.; Ogata, M. *Phys. Rev. B* **2008**, *77*, 195208.